Applied Catalysis B: Environment and Energy 382 (2026) 125942

Contents lists available at ScienceDirect

Applied Catalysis B: Environment and Energy

journal homepage: www.elsevier.com/locate/apcatb

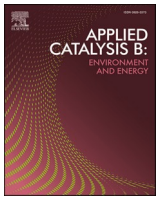

Effect of promoters (CeO_x, ZrO_x, and SiO_x) on activity and selectivity in the presence of H_2O for selective catalytic reduction (SCR) of NO with NH_3 by supported V_2O_5/TiO_2 catalysts

Dinh Nhat Dang Nguyen [a,1], Bar Mosevitzky Lis [a,b,1], Mingyu Guo [a,e,f,1], Wenda Hu [c,d,1], Nicholas R. Jaegers [c,d], Qingling Liu [e], Caixia Liu [e], Yong Wang [c,d,*], Jian Zhi Hu [c,d,*], Israel E. Wachs [a,**]

[a] Operando Molecular Spectroscopy & Catalysis Laboratory, Department of Chemical and Biomolecular Engineering, Lehigh University, Bethlehem, PA 18015, USA
[b] Department of Chemical Sciences and Bernal Institute, University of Limerick, Limerick V94 T9PX, Ireland
[c] Institute for Integrated Catalysis and Earth and Biological Science Directorate, Pacific Northwest National Laboratory, Richland, WA 99354, USA
[d] Voiland School of Chemical Engineering and Bioengineering, Washington State University, Pullman, WA 99163, USA
[e] Tianjin Key Laboratory of Indoor Air Environmental Quality Control, School of Environmental Science and Engineering, Tianjin University, Tianjin 300350, China
[f] Laboratory of Environmental Protection in Water Transport Engineering, Tianjin Research Institute of Water Transport Engineering, Tanggu, Tianjin 300456, China

ARTICLE INFO

Keywords:
Selective catalytic reduction
NO_x, supported V_2O_5/TiO_2
Promoters
Ligand effect
Spectroscopy
In situ
Raman
NMR
Infrared

ABSTRACT

A series of PO_x-promoted (P = Ce, Si, and Zr) TiO_2-supported vanadia catalysts were synthesized by incipient-wetness impregnation in order to examine the relationships between the anchoring sites, extent of oligomerization of the surface VO_x sites, nature and number of surface acid sites, and the NO/NH_3-SCR activity/selectivity under both *water vapor-free* and *water vapor-containing* reaction conditions at elevated temperatures. *In situ* IR spectroscopy showed that the deposited PO_x and VO_x species anchored at the support Ti-OH and P-OH/Ti-OH surface hydroxyls, respectively. *In situ* Raman spectroscopy revealed that all the oxides were essentially dispersed on the TiO_2 support as surface PO_x and VO_x sites under dehydrated conditions and reaction conditions. *In situ* solid-state ^{51}V MAS NMR revealed that the dehydrated surface VO_x sites are present as monomers, dimers, oligomers, and clusters, with comparable molecular distributions for the unpromoted and promoted catalysts. IR also revealed that the surface acid properties (surface NH_3* species on Lewis acid sites and surface NH_4^+* species on Brønsted acid sites) of the catalysts varied with the introduction of surface promoters and reaction conditions at elevated temperatures. Raman showed that the addition of vapor phase moisture to the SCR feed minimally perturbed the molecular structures of the surface VO_x sites. The SCR reaction rate, however, decreased because of the competitive adsorption between H_2O and NH_3/NO that also decreased the production of undesirable N_2O involving a bimolecular reaction. A correlation between SCR activity and nature and number of surface acid sites was not found to be present. The surface CeO_x promoter significantly increased the SCR activity because of its facile redox characteristic both as surface CeO_x sites on TiO_2 and bridging V-O-Ce bonds. In contrast, the surface ZrO_x and SiO_x sites on TiO_2 did not significantly affect the SCR activity because of their low redox propensity. The current studies demonstrate that the SCR activity is dominated by the redox properties of the promoter ligand V-O-P bonds and that the SCR selectivity to N_2O depends on the surface NH_3/NO/H_2O concentrations.

1. Introduction

Selective catalytic reduction (SCR) of nitrogen oxides (NO_x) using ammonia has been the leading engineering solution for the abatement of NO_x generated in combustion processes [1–3]. The supported V_2O_5/TiO_2 catalyst, the system of choice for power plants and industrial

* Corresponding authors at: Institute for Integrated Catalysis and Earth and Biological Science Directorate, Pacific Northwest National Laboratory, Richland, WA 99354, USA.
** Corresponding author.
E-mail addresses: yong.wang@pnnl.gov (Y. Wang), jianzhi.hu@pnnl.gov (J.Z. Hu), iew0@lehigh.edu (I.E. Wachs).
[1] Dinh Nhat Dang Nguyen, Bar Mosevitzky Lis, Mingyu Guo, and Wenda Hu contributed equally to this work.

https://doi.org/10.1016/j.apcatb.2025.125942
Received 21 May 2025; Received in revised form 3 September 2025; Accepted 6 September 2025
Available online 8 September 2025

boilers [4,5], is key for the NH_3-SCR process. While surface VO_x sites are considered to be the active sites, vanadia loading is typically limited to under 2 wt% V_2O_5 (~2.5 V atoms/nm^2) to limit the undesired oxidation of SO_2 to SO_3 [2,3,5–8]. The TiO_2 (anatase) support is typically chosen owing to the high dispersion of vanadia sites on the surface of the TiO_2 support [2,9,10], its low SO_2 oxidation propensity [2,10,11], its ability to rapidly reoxidize the VO_x active sites via a Mars-Van Krevelen mechanism [7,12], and the low propensity for surface VO_x to diffuse into the bulk lattice of the TiO_2 (anatase) support [13]. These features, coupled with its excellent thermal stability [2,14] and low cost [15,16], have led to the prevalent use of supported V_2O_5/TiO_2 catalysts in industrial applications in services where low temperature conversion is not needed.

The significant effect of water vapor on the catalytic activity and selectivity necessitates studying supported V_2O_5/TiO_2 catalysts under both *water vapor-free* and *water vapor-containing* conditions to better understand the effect of moisture since typical flue-gas streams of industrial boilers contain up to 20 % water vapor [17]. The presence of water vapor has been observed to impede NO conversion at water partial pressures above 1 % for the supported V_2O_5/TiO_2 catalysts [2,18], though this inhibiting effect saturates above 5 % water vapor [2,18]. The retarding effect of water has generally been suggested to arise from the suppression of the SCR reaction between adsorbed NH_3 with gas phase NO [19–22] or competitive adsorption with NH_3 [18,19,23–26]. At the same time, the undesirable N_2O generation from NH_3 over-oxidation at high temperatures [27] is also suppressed by water vapor in industrial combustion effluent.

Several promoters have been proposed to selectively enhance specific aspects of the supported V_2O_5/TiO_2 catalyst system [28–32], with the CeO_2, SiO_2, and ZrO_2 promoters having shown promise for enhancing SCR performance and stability. Ceria (CeO_2) can greatly improve the NH_3-SCR activity when incorporated before ($WO_3/V_2O_5/$-CeO_2/TiO_2) [28] or with (V_2O_5-WO_3-CeO_2/TiO_2) introduction of vanadia [33] due to both its inherent redox activity [34,35] and indirect promotional effects on the VO_x active sites [28,33]. Silicon dioxide (SiO_2) is another common promoter additive for supported V_2O_5/TiO_2 catalysts [29,32,36–41]. When SiO_2 is impregnated on the TiO_2 surface before the vanadia (V_2O_5/SiO_2-WO_3-TiO_2), the catalyst exhibits improved thermal stability and reduced TiO_2 anatase-rutile bulk phase transition [32,36], but also lower NO conversion compared to the SiO_2-free counterpart [36,39]. Impregnating ZrO_2 (V_2O_5-$ZrO_2/$-TiO_2-WO_3) increases the overall NH_3-SCR performance and enhances the catalyst's thermal stability despite the loss of Brønsted acid sites for NH_3 adsorption [31]. The various effects of the promoters (CeO_2, SiO_2, and ZrO_2) on NO conversion have been assigned primarily to ligand effects stemming from the anchoring of VO_x sites on these dispersed promoter oxides [28,29]. The effects of industrial-level water vapor on the surface VO_x molecular structures, surface acid sites and the NH_3-SCR performance, however, have not been examined in detail in prior studies.

In this study, incipient-wetness impregnated CeO_x-, SiO_x- and ZrO_x-promoted supported V_2O_5/TiO_2 catalysts were examined with *in situ* Infrared (IR) and *in situ* Raman spectroscopy to investigate the promoter oxide (PO_x) and VO_x anchoring sites, surface VO_x molecular structures and surface acid sites of the synthesized catalysts under *water vapor-free* and *water vapor-containing* reaction conditions. Although solid-state ^{51}V Magic Angle Spinning (MAS) Nuclear Magnetic Resonance (NMR) spectroscopy studies of supported vanadia catalysts have been extensively applied for almost 40 years to study the supported V_2O_5/TiO_2 catalysts to determine the molecular structures of the supported VO_x sites [7,42–49], the current study applies the ^{51}V MAS NMR spectroscopy method to determine the molecular structural changes of the surface vanadia sites of the dehydrated CeO_x-, SiO_x-, and ZrO_x-promoted supported V_2O_5/TiO_2 catalysts, which has never been done before. The findings were then compared with the SCR performance of the catalysts under steady state reaction conditions to yield insights into the structure-activity/selectivity relationships of the promoted supported V_2O_5/TiO_2 catalysts under industrially relevant reaction conditions.

2. Experimental

2.1. Catalyst synthesis

The TiO_2-supported catalysts were synthesized via the incipient-wetness impregnation method. Sub-monolayer loadings were used to avoid forming crystalline nanoparticles (NPs) at high surface coverage [5,50]. Zhu *et al.* reported that the dispersion capacity of surface CeO_x on a TiO_2 support is ~7 Ce ions/nm^2 [51]. Previous work has also indicated that monolayer dispersions of surface SiO_x and surface ZrO_x on TiO_2 supports were achieved at respective weight loadings of 6.2 % and 4.0 % (~12 atoms/nm^2) [52–54]. Initially, 80 % monolayer coverage of CeO_x (7.9 wt%, precursor: $Ce(NO_3)_3.6H_2O$ in DI water, 99.99 % Alfa Aesar), SiO_x (5.0 wt%, precursor: $Si(OC_2H_5)_4$ in ethanol, Sigma-Aldrich), and ZrO_x (3.2 wt%, 70 wt% $Zr(OCH_2CH_2CH_3)_4$ in n-propoxide, Alfa Aesar) were impregnated onto a TiO_2 support (Evonik P-25; ~55 m^2/g; ~80 % anatase and ~20 % rutile). A sample calculation of the 80 % monolayer for the CeO_x promoter is demonstrated in Equation S1. The moisture-sensitive SiO_x- and ZrO_x-promoted catalysts were synthesized in a glove box under an N_2 flow. The aqueous Ce $(NO_3)_3$ precursor was added to the TiO_2 in a drop-wise manner under constant stirring for 45 min. The samples were then dried overnight at room temperature, dehydrated under synthetic air (Airgas, flowing at 100 cc min^{-1}) at 120 °C for 2 hr, and calcined under synthetic air (Airgas, flowing at 100 cc min^{-1}) at 450 °C (heating at a rate of 1 °C min^{-1}) for 4 hr. Subsequently, the redox VO_x (1 wt%, precursor: NH_4VO_3 in DI water, 99.0 %, Alfa Aesar) was impregnated on the promoted TiO_2 supports and given the same drying and calcination procedures mentioned above.

2.2. Catalyst characterization

2.2.1. In situ diffuse reflectance infrared Fourier transform spectroscopy (DRIFTS)

In situ IR spectra were obtained using a Fourier-transform infrared (FTIR) spectrometer (Thermo NICOLET 8700) equipped with a high sensitivity mercury-cadmium-telluride (MCT-A) detector and a Harrick Praying Mantis Attachment (Model DRA-2) for diffuse reflectance spectroscopy. The powder catalysts were loaded into a customized corrosion-resistant Harrick Scientific cell (HVC-DRM-5 with Silcolloy 1000 coating), which was connected to a gas flow control system (Brooks Model 5850E). The reaction cell temperature was controlled with a Harrick ATC Temperature Controller unit (ATC02433667021701). The gases used in FTIR experiments were 40 % O_2/Ar (Linde AR OX40C-K), ultra high purity Ar (Airgas AR UHP300), 6000 ppm NH_3/Ar (Linde AR AM6000C-AS), and 6000 ppm NO/Ar (Linde AR NO6000C-AS). In each experiment, the catalyst was dehydrated at 500 °C (heating at a rate of 10 °C min^{-1}) for 1 hr under a gas mixture of 10 % O_2 (18.75 cc min^{-1} of 40 % O_2/Ar) and Ar (56.25 cc min^{-1} of Ar), after which the IR spectra were collected. Each catalyst was then cooled from 500 °C to 120 °C, under 10 % O_2/Ar (18.75 cc min^{-1} of 40 % O_2/Ar and 56.25 cc min^{-1} of Ar), and left to soak in inert Ar flow (75 cc min^{-1}) for 15 min. The IR spectra were collected using a 50 °C interval from 500 °C to 200 °C and at 120 °C. Finally, the reaction gas mixture was substituted for 10 % O_2/Ar and the catalyst was heated to 500 °C (heating at a rate of 10 °C min^{-1}) under SCR reaction conditions. For *water vapor-free* SCR conditions, the reaction gas mixture contained 1000 ppm NH_3 (12.5 cc min^{-1} of 6000 ppm NH_3/Ar), 1000 ppm NO (12.5 cc min^{-1} of 6000 ppm NO/Ar), 10 % O_2 (18.75 cc min^{-1} of 40 % O_2/Ar) and Ar (31.25 cc min^{-1}). For *water vapor-containing* SCR conditions, a reaction gas mixture of 1000 ppm NH_3 (12.5 cc min^{-1} of 6000 ppm NH_3/Ar), 1000 ppm NO (12.5 cc min^{-1} of 6000 ppm NO/Ar), 10 % O_2 (18.75 cc min^{-1} of 40 % O_2/Ar) and Ar (27.5 cc min^{-1})

was flown through a water bubbler containing DI water inside a water bath at 31 °C and atmospheric pressure. The resulting water content was ~5 molar %. The *in situ* IR spectra were collected at 120 °C and from 200 °C to 500 °C at 50 °C intervals. The intensities of the *in situ* IR spectra were normalized with respect to the TiO_2 support's IR band at 920 cm^{-1} as an internal standard using OMNIC 8.3.103 software designed for the NICOLET 8700 FTIR instrument. In this study, *in situ* DRIFTS spectra were collected under three conditions: dehydrated (no SCR reaction), SCR (*water vapor-free* SCR conditions), and SCR H_2O (*water vapor-containing* SCR conditions). The relative IR sensitivity of surface NH_4* species on Brønsted acid sites to surface NH_3* species on Lewis acid sites was close to unity [16], suggesting direct comparison between the population of these two adsorbed ammonia species can be conducted using their IR characteristic peaks. In this study, the calculation of the amount of adsorbed ammonia species is conducted using OMNIC 8.3.103 software after normalization of respective IR spectra with respect to the TiO_2 support's IR band at 920 cm^{-1}.

2.2.2. *In situ Raman spectroscopy*

In situ Raman spectra were obtained using a Horiba LabRAM HR Evolution spectrometer with visible wavelength laser excitation (532 nm). The laser was focused through a confocal microscope with a 50x objective (Olympus LMPLFLN50X) with 13.8 mW power at the sample. The Raman spectra were calibrated using a silicon standard with a reference band of 520.7 cm^{-1}. Powder samples were loaded into a corrosion-resistant cell (Harrick Scientific HVC, High-Temperature Reaction Chamber with CaF_2 windows and Silcolloy 1000 coating) and connected to a gas flow control system (Brooks Model 5850E). A Harrick ATC Temperature Controller unit (ATC02415713100901) controlled the sample temperature. The Raman spectra were collected with a 100 μm hole with a CCD camera detector (Horiba Synapse plus BIDD), resulting in a spectral resolution of ~1 cm^{-1}. The gases used in Raman experiments were 40 % O_2/Ar (Linde AR OX40C-K), ultrahigh purity Ar (Airgas AR UHP300), 6000 ppm NH_3/Ar (Linde AR AM6000C-AS), and 6000 ppm NO/Ar (Linde AR NO6000C-AS). The procedure for Raman spectral acquisition was as follows: catalyst dehydration was performed by flowing a gas mixture of 10 % O_2 (18.75 cc min^{-1} of 40 % O_2/Ar) and Ar (56.25 cc min^{-1}) at 400 °C for 30 min, under which the spectrum acquisition was collected. A subsequent spectrum was also taken after lowering the temperature to 120 °C under flowing 10 % O_2/Ar (18.75 cc min^{-1} of 40 % O_2/Ar and 56.25 cc min^{-1} Ar) and flushing with Ar (75 cc min^{-1}) for 15 min. Subsequently, the catalysts were exposed to the reaction gas mixture at 120 °C for 15 min before being heated to 200 °C. The sample was then gradually heated to 500 °C (heating at a rate of 10 °C min^{-1}). For *water vapor-free* SCR conditions, the reaction gas mixture contained 1000 ppm NH_3 (12.5 cc min^{-1} of 6000 ppm NH_3/Ar), 1000 ppm NO (12.5 cc min^{-1} of 6000 ppm NO/Ar), 10 % O_2 (18.75 cc of min^{-1} 40 % O_2/Ar) and Ar (31.25 cc min^{-1}). For *water vapor-containing* SCR conditions, a reaction gas mixture of 1000 ppm NH_3 (12.5 cc min^{-1} of 6000 ppm NH_3/Ar), 1000 ppm NO (12.5 cc min^{-1} of 6000 ppm NO/Ar), 10 % O_2 (18.75 cc min^{-1} of 40 % O_2/Ar) and Ar (27.5 cc min^{-1}) was flown through a water bubbler containing DI water inside a water bath at 31 °C and atmospheric pressure. The resulting water content was ~5 molar %. The Raman reaction spectra were taken at 120 °C and from 200 °C to 500 °C at 50 °C intervals. All the *in situ* Raman spectra intensities were normalized with respect to the TiO_2 support's Raman band at 150 cm^{-1} as an internal standard using the Horiba LabSpec 6.6.1.11 software designed for the Horiba LabRAM HR Evolution spectrometer. In this study, *in situ* Raman spectra are collected under three conditions: dehydrated (no SCR reaction), SCR (*water vapor-free* SCR conditions), and SCR H_2O (*water vapor-containing* SCR conditions).

2.2.3. *In situ solid-state ^{51}V MAS NMR spectroscopy*

The ^{51}V MAS NMR spectra were collected *in situ*, under controlled environmental conditions during acquisition that maintained samples in their pretreated states. Dehydrated catalyst samples were dried in flowing dry air (~20 cm^3 mg^{-1}) at 400 °C for 3 h. The samples were then sealed inside the thermal treatment tube with isolation valves and transferred to a dry N_2-purged glovebox (1 atm. total pressure) where the samples were loaded into 1.6 mm pencil-type ZrO_2 NMR rotors and sealed for NMR analysis.

All of the solid-state ^{51}V MAS NMR experiments were performed at room temperature on a Varian-Inova 600 MHz NMR spectrometer, operating at a magnetic field of 14.1 T. The corresponding Larmor frequency was 157.67 MHz. The ^{51}V spectra were acquired with a single pulse sequence with a 3π/16 pulse width of 2.85 μs and a spectral width of 5 MHz at a sample spinning rate of 34 kHz, using a 1.6 mm pencil-type MAS NMR probe. Depending on the sample, about 100,000 to 1,000,000 scans with a recycle delay time of 0.2 s and data acquisition time of 5 ms was employed. All the spectra were externally referenced using the center band of bulk V_2O_5 as the second reference, i.e., −613 ppm with respect to the common reference of $VOCl_3$ (0 ppm). While absolute quantitation is challenging due to the anisotropic line shapes and sideband intensity distributions, the reported relative signal intensities were based on consistent integration procedures across samples, with spectra acquired under identical pulse sequence conditions. This approach enables meaningful comparison of vanadium site distributions across the catalyst series.

2.3. *Steady state performance of the SCR catalysts*

Steady state reaction measurements were conducted using an online Gasmet DX4000 FTIR Gas Analyzer, specifically designed for monitoring the emissions of NO_x. The reactor device was manufactured by Beijing Tongshenglida Technology Co. Ltd. Before the measurement, the gas analyzer was calibrated to generate a standard concentration curve for each reactant gas, which was later applied to quantify the measured results. Regarding the experimental protocol, approximately 120 mg of each catalyst was placed in a furnace supplied by Longkou Xianke Instrument Co. Ltd, heated to 400 °C (at a rate of 20 °C min^{-1}), held for 30 min, and cooled down to 100 °C under pure O_2 flow (50 cc min^{-1}) to dehydrate it. Subsequently, the reaction gases (total flow of 300 cc min^{-1}) were introduced into the system. The compositions of the reaction gases were as follows: 1000 ppm NO/1000 ppm NH_3/10 % O_2/N_2 for *water vapor-free* SCR conditions and 1000 ppm NO/1000 ppm NH_3/10 % O_2/~5 % H_2O/N_2 for *water vapor-containing* SCR conditions. The O_2 and N_2 were pure gases, while NO and NH_3 were 1 % with N_2 balance. All gases were supplied by Yancheng Zhengda Chemical Co. Ltd. The H_2O was introduced into the reaction by bubbling the gases through the water bath at 31 °C and atmospheric pressure. The NO, NO_2, N_2O, and NH_3 concentrations were recorded at 100, 200, 250, 300, 350, 400, and 500 °C (heating at a rate of 10 °C min^{-1}). The data was collected 30 min after the reaction at each temperature. The N_2O formation graphs were plotted on the same scale for comparison.

3. Results and discussion

3.1. *Anchoring sites of supported PO_x promoters and surface VO_x sites on the TiO_2 support*

The PO_x promoters and VO_x sites anchor by titrating surface hydroxyls on the oxide support [28,29]. The TiO_2 support possesses both more acidic bridging Ti-(OH)-Ti (3630, 3660 and 3674 cm^{-1}) and more basic terminal Ti-(OH) (3710 cm^{-1}) surface hydroxyls [16,55]. Impregnation of 1 % V_2O_5 on the unpromoted TiO_2 support (20 % monolayer surface VO_x coverage for the current TiO_2 support (Evonik P-25)) selectively titrates the terminal Ti-(OH) and some of the bridging Ti-(OH)-Ti (3674 cm^{-1}) surface hydroxyls, while also forming new surface V-(OH)-Ti (3640 cm^{-1}) surface hydroxyls [28,29]. Anchoring of 5 % SiO_2 onto the TiO_2 support (80 % monolayer surface SiO_x coverage) generates terminal surface Si-(OH) (3660 and 3773 cm^{-1}) surface hydroxyls [29]. The lack of IR detectable titration of the Ti-(OH)-Ti and

Ti-(OH) surface hydroxyls is attributed to the overlap of the surface SiO_x and TiO_2 surface hydroxyls [29]. Anchoring of 1 % VO_x on the surface modified SiO_x/TiO_2 support consumes both the Si-OH and Ti-(OH)-Ti surface hydroxyls and does not generate new detectable surface hydroxyls [29]. Anchoring of 3.2 % ZrO_2 onto the TiO_2 support (80 % monolayer surface ZrO_x coverage for the current TiO_2 support (Evonik P-25)) forms both terminal Zr-(OH) (3750 cm^{-1}) and bridging Zr-(OH)-Zr (3710 and 3664 cm^{-1}) surface hydroxyls [29]. The lack of IR detectable titration of the Ti-(OH)-Ti and Ti-OH surface hydroxyls is attributed to the overlap of the surface ZiO_x and TiO_2 surface hydroxyls [29]. Impregnation of 1 % V_2O_5 on the promoted ZrO_x/TiO_2 support titrates all the types of surface hydroxyls (Zr-(OH)-Zr, Zr-(OH), Ti-(OH)-Ti and Ti-(OH)) present in this catalyst [29]. Anchoring of 7.9 % CeO_2 onto TiO_2 support (80 % monolayer surface CeO_x coverage for the current TiO_2 support (Evonik P-25)) titrates the Ti-(OH)-Ti (3661 and 3630 cm^{-1}) surface hydroxyls and generates Ce-(OH) (3710 cm^{-1}) surface hydroxyls [28]. Impregnation of 1 % V_2O_5 on the surface modified CeO_x/TiO_2 support titrates all the Ce-(OH) and Ti-(OH) surface hydroxyls [28]. The lack of IR detectable titration of the Ti-(OH)-Ti and Ce-(OH)-Ce surface hydroxyls is attributed to the overlap of the surface CeO_x and TiO_2 hydroxyls [28]. In summary, (1) the extensive titration of the surface hydroxyls on the TiO_2 support by the promoter oxides reflects the two-dimensional nature of the promoters on the TiO_2 support and (2) the surface VO_x sites extensively anchor at both the oxide promoter surface hydroxyls, generating unique V-O-P ligands (P = Ce/Si/Zr), and also at the TiO_2 surface hydroxyls [28,29], presumably also forming mixed bridging surface V-O-Ti/P sites [56].

3.2. *In situ* Raman spectroscopy of unpromoted and promoted supported catalysts

Although the current TiO_2 support (Evonik P-25) consists of bulk ~80 % anatase and ~20 % rutile phases, the TiO_2 anatase bands (150, 201, 395, 510, and 631 cm^{-1}) [57,58] dominate the *in situ* Raman spectra (Fig. S1) due to the higher light-scattering efficiency of the anatase phase compared to the rutile phase. The absence of Raman vibrations from crystalline CeO_2 (464 cm^{-1}) [35,59], crystalline SiO_2 (970 cm^{-1}) [60], and crystalline ZrO_2 (330 and 469 cm^{-1}) [61,62] nanoparticles (Fig. S1) indicates that these oxide promoters are fully dispersed on the TiO_2 support as two-dimensional surface oxide overlayers. The lack of Raman bands for crystalline V_2O_5 (997 cm^{-1}) [63] nanoparticles in conjunction with the presence of Raman bands for the dehydrated surface VO_x sites (1029 cm^{-1}) [5,64–66] (Fig. 1) confirms the complete dispersion of the surface VO_x sites on the TiO_2 support [5]. Moreover, there are no Raman bands indicative of crystalline bulk $CeVO_4$ (860 cm^{-1}) [67,68] and bulk ZrV_2O_7 (769 cm^{-1}) [69]

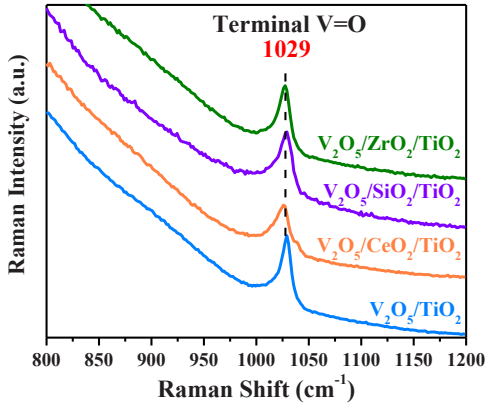

Fig. 1. *In situ* Raman spectra of dehydrated unpromoted and promoted supported 1 % $V_2O_5/PO_x/TiO_2$ catalysts at 400 °C for the region 800–1200 cm^{-1} spectral region.

nanoparticles on the promoted catalysts, demonstrating that these nanoparticles are not present on the promoted catalysts. Furthermore, the *in situ* Raman spectra of the dehydrated surface VO_x sites on the unpromoted and promoted catalysts (Fig. 1) are rather similar, which reflects no significant variation in the terminal V=O bond vibration (~1029 cm^{-1}) of the dehydrated surface VO_x sites as probed by Raman spectroscopy.

The vibrations of the terminal V=O bonds, however, were affected by the presence of water vapor and SCR reaction conditions from 120 to 300 °C resulting from hydrogen bonding of adsorbed H_2O and NH_3 with the V=O bonds, which manifests as a ~5–10 cm^{-1} redshift and broadening of the terminal V=O vibrational band (see IR and Raman spectra of Figs. S2-S6). The influence of H-bonding was minimal at 400–500 °C SCR reaction conditions since the surface concentrations of adsorbed H_2O and NH_3 are small at these elevated reaction temperatures. It can, thus, be surmised that the nature of the surface VO_x sites on the TiO_2 and surface modified PO_x/TiO_2 supports at elevated temperatures are very similar under dehydrated and SCR reaction conditions.

3.3. *In situ* solid-state ^{51}V MAS NMR spectroscopy of dehydrated supported VO_x catalysts

Previous *in situ* solid-state ^{51}V MAS NMR studies on the TiO_2 support with the same surface VO_x concentration (1 V/nm^2) as in the present study revealed a wide range of surface VO_x structures under dehydrated conditions [7]. All examined catalysts were shown to contain less than 1 % of reduced vanadium V^{4+} when probed with Electron Paramagnetic Resonance (EPR) spectroscopy [7], indicating essentially fully oxidized vanadia sites following the dehydration protocols for the *in situ* NMR measurement. For the dehydrated supported 1 %V_2O_5/TiO_2 catalyst (Fig. 2), the *in situ* ^{51}V MAS NMR signals associated with monomeric surface VO_x sites (-505 and −531 ppm) accounted for 32 % of all vanadia spins, dimeric surface VO_x sites (-561 and −581 ppm) accounted for 44 % of the total vanadia spins, oligomeric surface VO_x sites (-646 and −682 ppm) represented 15 % of the total detected spins, and 12 % of the detected vanadia sites (-610 ppm) were attributed to bulk V_2O_5, which was not detected using *in situ* Raman spectroscopy and may represent an oligomeric surface VO_x molecular structure that is similar to V_2O_5 [7,8]. The assignments of the ^{51}V chemical shifts with respect to monomeric, dimeric, and oligomeric surface VO_x species were proposed in previous publications and supported by DFT calculations [7,70]. With a similar approach pursued herein, the *in situ* solid-state ^{51}V MAS NMR spectra of the dehydrated promoted (CeO_x, SiO_x, and ZrO_x) supported VO_x/TiO_2 catalysts are presented in Fig. 2.

3.3.1. *Supported 1 % V_2O_5/7.9 % CeO_2/TiO_2*

The *in situ* solid-state ^{51}V MAS NMR spectrum of the dehydrated supported 1 % V_2O_5/7.9 % CeO_2/TiO_2 catalyst (Fig. 2) exhibits a wide range of ^{51}V spins. Two features from monomeric surface VO_x sites are present at −518 ppm (7 % of all V^{5+} sites) and −544 ppm (21 % of all V^{5+} sites), suggesting the presence of distorted VO_4 and VO_5 square pyramidal-like structures, respectively [49]. The ^{51}V NMR peak at −567 ppm (11 % of total V^{5+} sites) is associated with dimeric surface VO_x sites [7,49], but the contribution from distorted V-O-V chains within the surface VO_x structures [71] cannot be neglected. A second dimeric surface VO_x site (-589 ppm) accounts for almost half of the total oxidized surface vanadia pool (47 % of all V^{5+} sites). The ceria-promoted catalyst shows a higher population of dimeric surface vanadia sites than the unpromoted catalyst (58 % and 44 %, respectively), which suggests ceria stabilizes surface VO_x dimer sites. The ^{51}V NMR peak at −621 ppm has been suggested to be surface vanadia oligomers [7,70] and appears to have overshadowed the band of V_2O_5 nanoparticles (-614 ppm). A higher isotropic shift is absent for oligomeric vanadia species at −648 ppm [7]. Additionally, signals corresponding to the bulk $CeVO_4$ phase (-427 ppm) and distorted surface VO_4 sites (-750 ppm) [71] are not detected, suggesting the absence of these

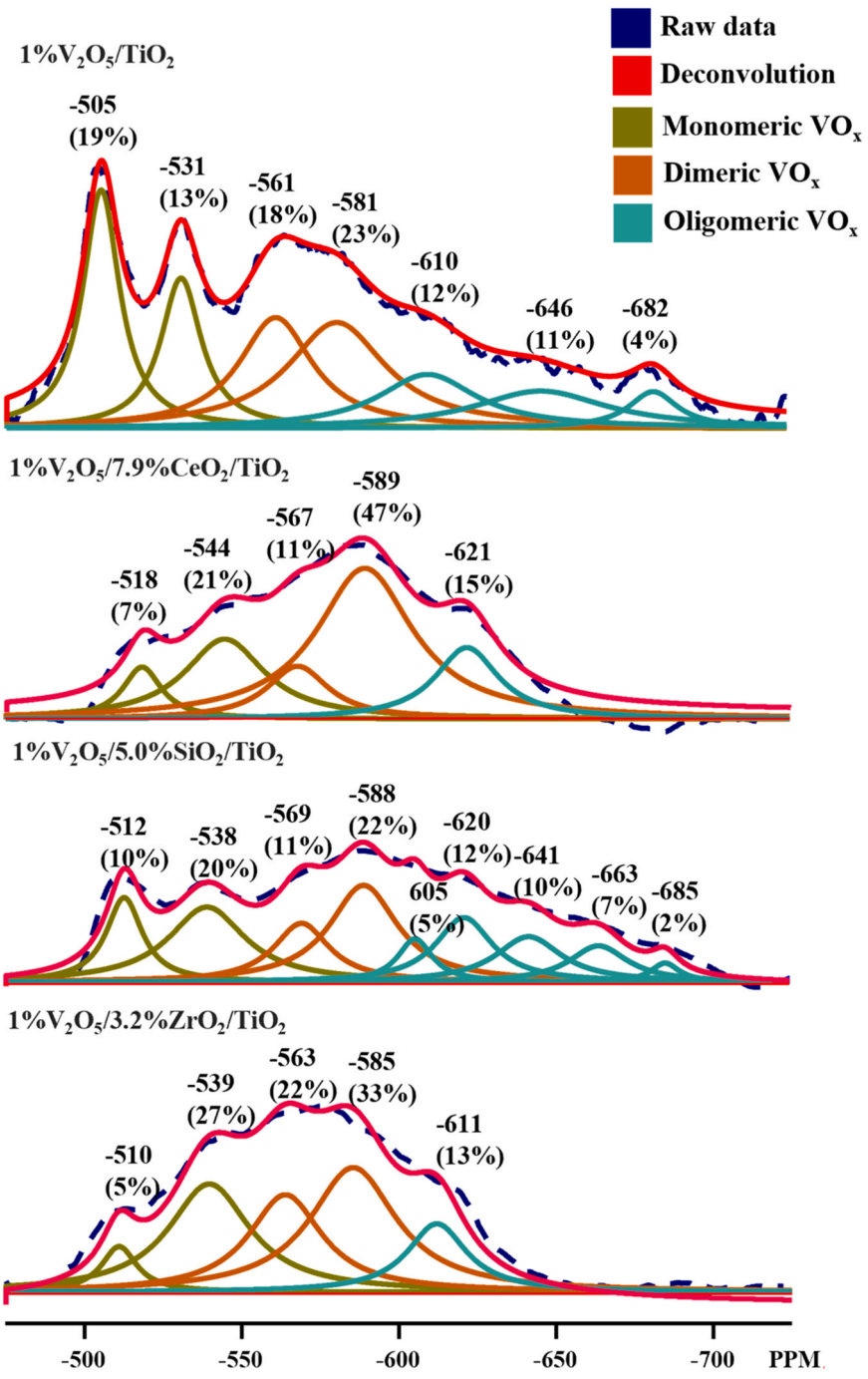

Fig. 2. *In situ* solid-state ^{51}V MAS NMR spectra of dehydrated unpromoted and promoted titania-supported vanadia catalysts and their spectral deconvolution.

structures in the supported 1 % V_2O_5/7.9 % CeO_2/TiO_2 catalyst. Overall, there is a shift from monomeric surface VO_x to dimeric and oligomeric surface VO_x sites when the surface of the TiO_2 support is modified with surface CeO_x sites (see Table 1).

3.3.2. *Supported 1 % V_2O_5/5.0 % SiO_2/TiO_2*

The *in situ* solid-state ^{51}V MAS NMR spectrum of the dehydrated supported 1 % V_2O_5/5.0 % SiO_2/TiO_2 catalyst (Fig. 2) exhibits the largest variation of surface VO_x sites of all the examined supported vanadia catalysts. Monomeric surface vanadia sites (-512 and −538 ppm) occupy about one-third of the total vanadia spins and two dimeric species (-569 and −588 ppm) make up a similar percentage. The ^{51}V NMR peaks at −620 ppm and −641 ppm suggest the presence of similar oligomeric vanadia structures as for the ceria-promoted and unpromoted catalysts, respectively. The feature at −605 ppm may be related to a trace of crystalline V_2O_5 nanoparticles [72] or oligomeric surface VO_x sites with a similar coordination [7]. The two vanadia features at −663 and −685 ppm have not been previously reported for silica-promoted TiO_2-supported vanadium oxide catalysts. They are likely associated with oligomeric vanadia species since surface vanadia oligomers typically exhibit NMR bands above −600 ppm. Previous ^{51}V MAS NMR measurements demonstrated a unique broad feature at −675 ppm representing surface vanadia sites for the supported V_2O_5/SiO_2 catalysts without conclusive evidence of what vanadia sites were present [72,73]. The absence of the ^{51}V NMR peak at −675 ppm for the supported V_2O_5/SiO_2/TiO_2 catalysts indicates that such a surface

Table 1
Summary of *in situ* solid-state ^{51}V MAS NMR chemical shifts (ppm) with respect to surface vanadia concentration for each dehydrated unpromoted and promoted supported 1 % V_2O_5/TiO_2 catalysts. Fractions are obtained from deconvolution of ^{51}V MAS NMR spectra. 5–15 % quantitative errors reflect the combined effects of spectral noise/model variance, imperfect central-transition selectivity, and the absence of T_1 corrections [75,76].

Structures	1 % V_2O_5/TiO_2	1 % V_2O_5/ 7.9 % CeO_2/ TiO_2	1 % V_2O_5/ 5.0 % SiO_2/ TiO_2	1 % V_2O_5/ 3.2 % ZrO_2/ TiO_2
Monomer	32 %	28 %	30 %	32 %
Dimer	41 %	58 %	33 %	55 %
Oligomer & Bulk like VO_x	27 %	15 %	36 %	13 %

VO_x structure is not present on this catalyst. Overall, there is a shift from monomeric surface VO_x to oligomeric surface VO_x sites when the TiO_2 support is surface modified with surface SiO_x sites (see Table 1).

3.3.3. Supported 1 % V_2O_5/3.2 % ZrO_2/TiO_2

The *in situ* solid-state ^{51}V MAS NMR spectrum of the dehydrated supported 1 % V_2O_5/3.2 % ZrO_2/TiO_2 catalyst (Fig. 2) shows a strong resemblance to the spectrum of the ceria-promoted $V_2O_5/CeO_2/TiO_2$ catalyst. The two structures of monomeric surface vanadia sites (-510 and −539 ppm) account for 32 % of the total V^{5+} sites. The isotropic chemical shifts of dimeric surface vanadia sites at −563 and −585 ppm indicate that these surface vanadia sites make up more than half (55 %) of the total surface vanadia sites. The ^{51}V NMR peak at −611 ppm (accounting for 13 % of detected surface V^{5+} sites) has been ascribed to bulk crystalline V_2O_5 or oligomeric surface VO_x sites with a similar coordination [7]. The ^{51}V NMR peak for oligomeric surface VO_x structures (around −621 ppm) is absent from the ^{51}V NMR spectrum of the dehydrated supported 1 % V_2O_5/3.2 % ZrO_2/TiO_2 catalyst. Overall, there is a shift from monomeric surface VO_x to dimeric surface VO_x sites when the TiO_2 support is surface modified with surface ZrO_x sites (see Table 1).

3.3.4. Summary of dehydrated *in situ* ^{51}V MAS NMR spectra

The distribution of dehydrated surface vanadia structures for the unpromoted and promoted supported 1 % V_2O_5/TiO_2 catalysts, as determined with *in situ* solid-state ^{51}V MAS NMR, is summarized in Table 1. There is a shift from monomeric to dimeric- (CeO_x and ZrO_x) and oligomeric-rich (SiO_x) surface VO_x sites for all the promoted supported 1 % V_2O_5/TiO_2 catalysts relative to the unpromoted catalyst. The V_2O_5 nanoparticles are essentially absent from the unpromoted catalyst and promoted 1 % V_2O_5/TiO_2 catalysts. The surface VO_x sites, when promoted with SiO_x, exhibit a more uniform distribution among the surface VO_x structures (see Fig. 1) in comparison to promotion with CeO_x and ZrO_x, which possess more than 50 % surface VO_x dimers, and unpromoted 1 % V_2O_5/TiO_2, which possesses mostly monomeric and dimeric surface VO_x sites. These findings reveal how the specific dispersed surface PO_x sites [28,29] influence the molecular structures of the dehydrated surface VO_x sites on the TiO_2 support by modifying the available anchoring surface hydroxyls on the titania support.

In situ Raman spectroscopy reveals that the surface VO_x structures at SCR at elevated reaction temperatures are similar to the dehydrated surface VO_x sites rather than the hydrated surface VO_x sites at lower temperatures [74]. This occurs because the surface concentration of water is low at elevated SCR reaction temperatures. Only at lower temperatures (<200 °C), which is much lower than the SCR reaction temperatures, does moisture condense on the catalyst surface and alter the surface VO_x structures by hydration. ^{51}V MAS NMR spectra of the hydrated catalysts and their detailed structural analyses are provided in the SI section. Note, however, that the hydrated surface VO_x structures are not related to the high temperature SCR reaction where condense water is absent and, thus, are not included in the main text. The supported VO_x sites do show the sensitivity of the surface VO_x sites to condensed water, which confirms the two-dimensional nature of the dehydrated surface VO_x sites on the TiO_2 support and absence of 3D nanocrystalline phases (e.g., V_2O_5).

3.4. Surface acidity under SCR reaction conditions

Water Vapor-Free SCR. In situ IR with ammonia adsorption was employed to chemically probe the dynamics of the Lewis and Brønsted acid surface sites under *water vapor-free* SCR reaction conditions, as shown in Fig. 3. Both Lewis and Brønsted acid surface sites are present on the unpromoted supported 1 % V_2O_5/TiO_2 catalyst under *water vapor-free* SCR conditions at 1175–1180 cm^{-1} for surface NH_3* [77–79] and 1427 cm^{-1} for surface NH_4^{+*} species [77,80] (Fig. S10a), respectively. The IR intensities of the Lewis and Brønsted surface ammonia species decrease with increasing temperature due to increased SCR reaction rates, accelerated NH_3 desorption rates, and decreased NH_3 adsorption rates. With increasing temperature, for the unpromoted supported 1 % V_2O_5/TiO_2 catalyst, the IR band for surface NH_3* species on Lewis acid sites slightly blueshift from 1175 to 1180 cm^{-1} (Fig. S10a), reflecting an increase in the acid strength of the surface NH_3* species at 300 °C, while the IR band for the surface NH_4^{+*} species on Brønsted acid sites remains constant at 1427 cm^{-1} in the 120–300 °C temperature range (Fig. S10a) before diminishing at 400 °C (Fig. 3b). At 400–450 °C, the concentrations of Lewis NH_3* and Brønsted NH_4^{+*} surface species on the catalytic surface are significantly reduced and no longer detectable with FTIR (Fig. 3a,b). Moreover, the surface NH_4^{+*} species from the Brønsted acid sites desorb at lower temperatures than the surface NH_3* species from the Lewis acid sites [28,29]. Therefore, it is reasonable to expect a higher concentration of the surface NH_3* species on the Lewis acid sites than surface NH_4^{+*} on the Brønsted acid sites at a given reaction temperature under *water vapor-free* SCR reaction conditions (Table S2). The *in situ* IR spectra for the promoted supported 1 % V_2O_5/TiO_2 catalysts (Fig. S10b-d) exhibit the same general behavior of the surface NH_3* and NH_4^{+*} species on Lewis and Brønsted acid sites, respectively, as the unpromoted catalyst. As temperature rises from 120 °C to 300 °C, the IR spectra of surface NH_3* species on Lewis acid sites exhibit a slight blueshift for the CeO_x- and ZrO_x-promoted catalysts (1175–1183 cm^{-1}) (Fig. S10b,d), reflecting an increase in the acid strength of the surface NH_3* species at 300 °C. The IR spectra of the surface NH_4^{+*} species on Brønsted acid sites of the CeO_x- and ZrO_x-promoted catalysts, however, are essentially unperturbed and appear at 1427 cm^{-1} (Fig. S10b,d). The SiO_x-promoted catalyst, however, does not indicate the presence of any surface NH_3* species on Lewis acid sites at all reaction temperatures [29], and only exhibits the IR band for surface NH_4^{+*} species on Brønsted acid sites at 1427 cm^{-1} (Fig. S10c). At 450 °C, the IR bands of Lewis acid sites of all the promoted catalysts are no longer detectable due to their low surface concentration (Fig. 3a). In contrast, the surface NH_4^{+*} species on the Brønsted acid sites of CeO_x- and ZrO_x-promoted catalysts diminish at much lower temperatures of 200 and 250 °C, respectively (Fig. 3b). Only the SiO_x-promoted catalyst exhibits the presence of surface NH_4* species on Brønsted acid sites at 350 °C (Fig. 3b). This indicates that the SiO_x-promoted catalyst possesses Brønsted acid sites with stronger acid strength compared to the other catalysts. When the temperature is lowered from 500 to 400 °C, the amount of surface NH_3* species on Lewis acid sites exhibits the following order: unpromoted > ZrO_x-promoted > CeO_x-promoted >> SiO_x-promoted (Fig. 3a), while the amount of surface NH_4* species on Brønsted acid sites exhibits the following order: SiO_x-promoted >> unpromoted ~ CeO_x-promoted ~ ZrO_x-promoted (Fig. 3b). Collectively, the surface PO_x promoters decreased the number of surface Lewis acid sites, with surface SiO_x completely suppressing the Lewis acid sites, and minimally perturbed the number of surface Brønsted acid sites, with surface SiO_x increasing the number of Brønsted acid sites under *water vapor-free* SCR reaction conditions.

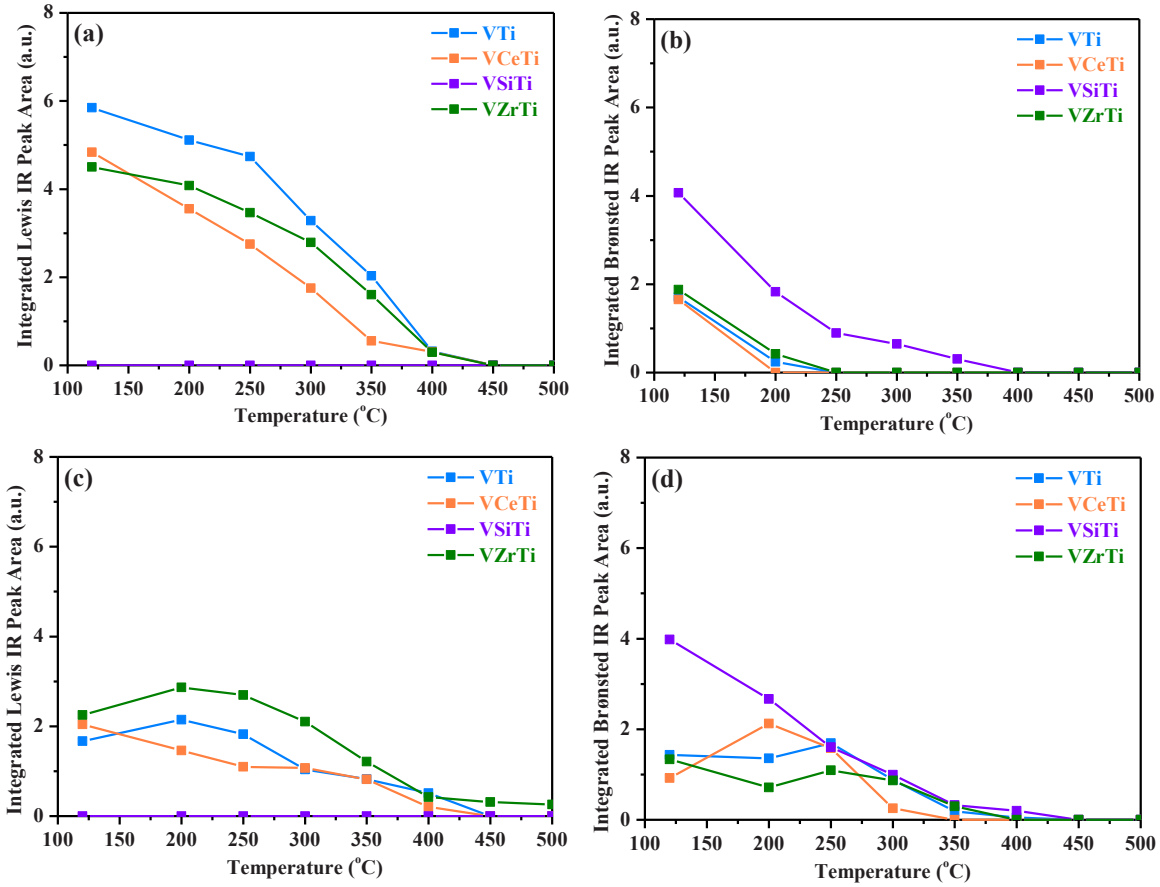

Fig. 3. Effect of SCR reaction temperature on the amount of surface Lewis and Brønsted acid sites as probed with *in situ* IR measurements under (a,b) *water vapor-free* SCR reaction (10 % O_2/1000 ppm NO/1000 ppm NH_3/Ar) and (c,d) *water vapor-containing* SCR reaction (10 % O_2/1000 ppm NO/1000 ppm NH_3/5 % H_2O/Ar).

Water Vapor-Containing SCR. The presence of ~5 % H_2O in the SCR feed stream affects the surface acidity properties of the TiO_2-supported catalysts. The intensity of the IR bands of the surface NH_3* species on Lewis acid sites (~1200 cm^{-1}) and surface NH_4^{+*} species on Brønsted acid sites (1427 cm^{-1}) are significantly diminished for both unpromoted and promoted supported 1 % V_2O_5/TiO_2 catalysts (Fig. 3c). A blueshift of the IR band of the surface NH_4^{+*} species on Brønsted acid sites from 1427 to 1435 cm^{-1} is observed (Fig. S11), reflecting an increase in the acid strength of the surface NH_4^{+*} species for all catalysts under the *water vapor-containing* SCR reaction environment. This is related to the conversion of surface NH_3* to NH_4^{+*} species in the presence of water vapor [16]. The intensity of the IR bands of surface NH_3* species on Lewis acid sites are extensively diminished for all examined catalysts (Fig. 3c). The surface NH_4^{+*} species on Brønsted acid sites are present in all the catalysts under the *water vapor-containing* SCR reaction conditions (Fig. 3d) and exhibit higher intensities of the IR bands relative to those under *the water vapor-free* SCR reaction conditions (Fig. 3b), indicating an increase in the number of the surface NH_4^{+*} species on the catalyst surface under the *water vapor-containing* SCR reaction environment. The IR bands for the surface NH_4^{+*} species on Brønsted acid sites of both unpromoted and promoted catalysts (Fig. 3d) diminish at 450 °C. At temperatures lower than 400 °C under the *water vapor-containing* SCR reaction conditions, the amount of surface NH_3* species on Lewis acid sites follows the order: ZrO_x-promoted > unpromoted > CeO_x-promoted >> SiO_x-promoted (Fig. 3c). The corresponding trend of the surface NH_4^{+*} species on Brønsted acid sites follows the sequence: SiO_x-promoted > unpromoted > ZrO_x-promoted > CeO_x-promoted (Fig. 3d). These results demonstrate conversion of surface NH_3* to NH_4^{+*} species in the presence of water vapor in agreement with prior publications [18,19,23–26]. The extent of decrease in total surface acid sites, however, varies with the specific surface PO_x promoter. The unpromoted and redox (CeO_x-) promoted catalysts are more sensitive to the inhibition effect than the non-redox (ZrO_x-) promoted catalyst (Table S2 and S3). The exception is the SiO_x-promoted catalyst that exhibits somewhat similar concentrations of Brønsted acid sites and no Lewis acid sites under both *water vapor-free* and *water vapor-containing* SCR reaction environments (Table S2 and S3), which reflects the hydrophobic nature of the SiO_x--surface modified TiO_2 support. These results demonstrate that the number, strength, and stability of the surface acid sites of the supported 1 % V_2O_5/TiO_2 catalyst are significantly influenced by the surface PO_x promoters on the TiO_2 support and the presence of water vapor in the feed.

3.5. Steady state SCR performance of unpromoted and promoted supported $VO_x/PO_x/TiO_2$ (P = Ce, Si, Zr) catalysts

Water Vapor-Free SCR. The unpromoted and promoted supported 1 % V_2O_5/TiO_2 catalysts were investigated for the NO and NH_3 SCR activity and N_2O selectivity during the steady state reaction (see Fig. 4 and S12) between 100 and 500 °C. The unpromoted supported 1 % V_2O_5/TiO_2 catalyst becomes SCR-active at 200 °C and reaches its maximal NO conversion (76 %) at 400 °C (Fig. 4a). The conversion of NO experiences a slight decrease above 400 °C due to over-oxidation of the reducing NH_3 needed for the SCR reaction [27]. The CeO_x-promoted catalyst becomes SCR-active above 100 °C and achieves higher NO conversion (90 %) at 400 °C. Additionally, the redox CeO_x-promoted catalyst maintains the highest NO conversion over a broad temperature range (200–400 °C) compared to the other catalysts (Fig. 4a). The promotional effect of the CeO_x-promoted catalyst is attributed to the combined redox activity by the CeO_x and the CeO_x-promoted surface VO_x sites [28]. To

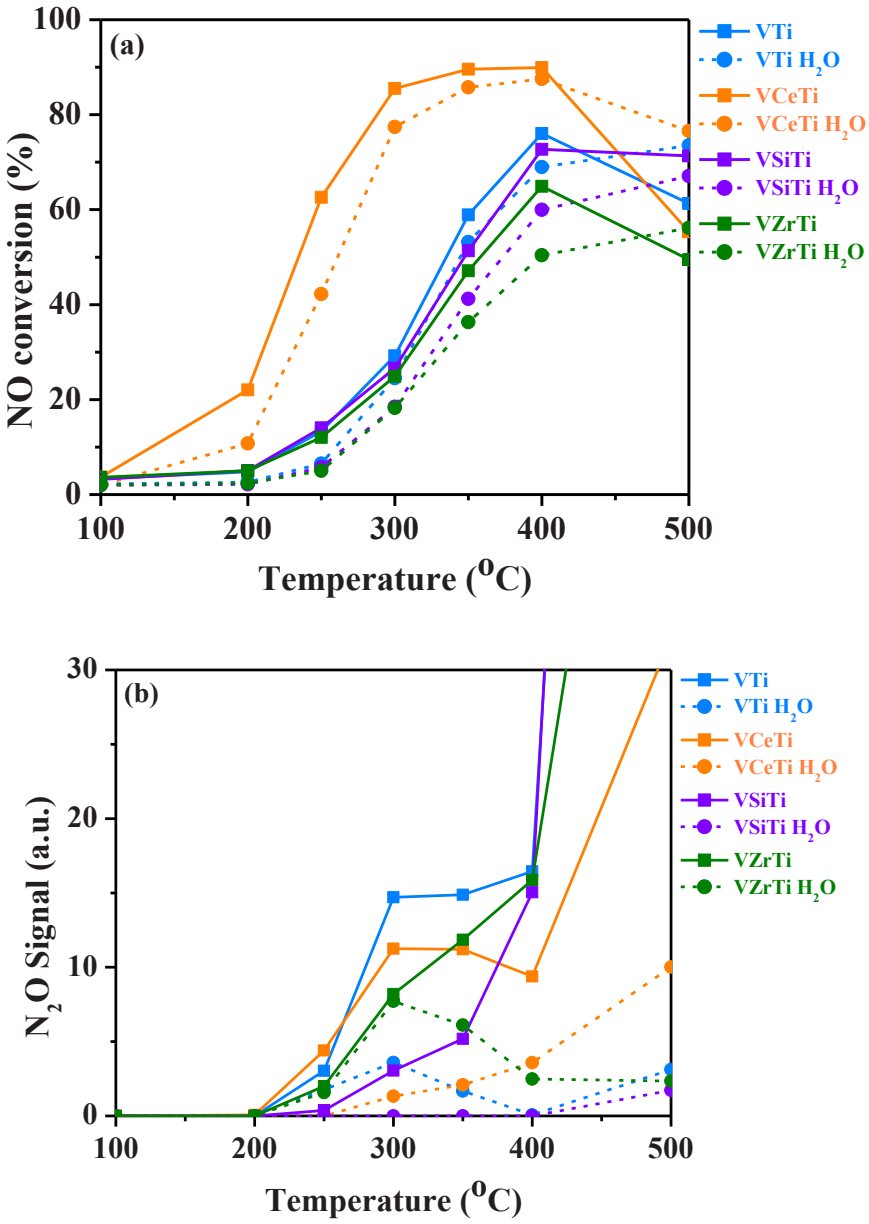

Fig. 4. Comparison of steady state kinetic data of unpromoted and promoted catalysts for (a) NO conversion and (b) N_2O formation. Reaction gas compositions include 10 % O_2/1000 ppm NO/1000 ppm NH_3/N_2 for *water vapor-free* SCR reaction conditions and 10 % O_2/1000 ppm NO/1000 ppm NH_3/5 % H_2O/N_2 for water vapor-containing SCR reaction conditions. The straight lines (*water vapor-free*) and dashed lines (water vapor) were constructed to aid the visualization of the data and were not measured data points.

further illustrate the promotional aspect of the CeO_x-sites, the steady state SCR performance of the PO_x-promoted TiO_2 catalysts (without VO_x sites) is examined in Figure S13. The CeO_x/TiO_2 catalyst exhibits enhanced SCR activity, while the SiO_x/TiO_2 and ZrO_x/TiO_2 catalysts demonstrate almost no SCR activity ($CeO_x >> ZrO_x \sim SiO_x$). The improved promotion of CeO_x-containing catalysts for NO_x conversion has previously been reported for the TiO_2, VO_x/TiO_2, and WO_x/TiO_2 catalyst systems [34,81–83]. At 500 °C, the NO conversion of the CeO_x-promoted catalyst decreases due to over-oxidation of NH_3, dropping to 55 % NO conversion compared to 60 % of the unpromoted catalyst (Fig. 4a). The ZrO_x-promoted catalyst (Fig. 4a) shows a moderately lower maximal NO conversion (65 %) than the unpromoted catalyst over the examined temperature range of 100–500 °C and exhibits the lowest NO conversion among the catalysts. The conversion of NO by the SiO_x-promoted catalyst (Fig. 4a) exhibits a comparable NO conversion to the unpromoted catalyst with only a slightly lower maximum value of 73 % at 400 °C. The similar SCR activity of the SiO_x-promoted catalyst compared to the unpromoted catalyst was also previously found for the supported V_2O_5/WO_3–TiO_2 and V_2O_5/WO_3/-TiO_2 catalysts [37–39,84]. Noticeably, the SiO_x promotion enhances the catalyst's resistance to NH_3 over-oxidation and exhibits approximately the same NO conversion (71 %) at 500 °C and (73 %) at 400 °C. In general, the order of NO conversion for all the catalysts can be summarized as follows: CeO_x-promoted > > unpromoted > SiO_x-promoted > ZrO_x-promoted. Previous studies suggested the ligand bonds (V-O-P, P = Ce, Si, Zr) to be responsible for controlling the redox activity of the anchored surface VO_x sites [28,29], which are the active sites for the SCR reaction on the supported V_2O_5/TiO_2 catalysts [5,7,16]. The slightly comparable SCR activities of the unpromoted, SiO_x-promoted, and ZrO_x-promoted catalysts, however, suggest that the surface VO_x sites are mostly preferentially anchored at the exposed surface TiO_x sites of the support and possibly also possess similar surface VO_x structures.

The formation of N_2O increases with temperature from 200 to 500 °C under the *water vapor-free* SCR reaction conditions for all the examined catalysts (Fig. 4b). The unpromoted supported 1 % V_2O_5/TiO_2 generates the highest N_2O level between 200 and 400 °C, which is only surpassed by the SiO_x-promoted catalyst at 500 °C (Fig. S12), with the other surface PO_x promoters mildly suppressing N_2O formation (Fig. 4b). The N_2O formation exhibits the following trend: unpromoted > CeO_x-promoted > ZrO_x-promoted > SiO_x-promoted in the 250–350 °C temperature range. The N_2O generation propensity was previously shown to be inversely correlated with the strength of Brønsted acid sites [28,29] from inhibition by the stronger acid sites involved in the rate-determining step of N_2O production [27]. The N_2O generation trends herein demonstrate the same inverse correlation with the order of Brønsted acid strength, SiO_x-promoted > ZrO_x-promoted > CeO_x-promoted > unpromoted (Table S2), in the 250–350 °C temperature range under the *water vapor-free* SCR reaction conditions. The stronger acid sites in SiO_x- and ZrO_x-promoted catalysts may suppress the further oxidation of the NH_2- group in the [NH_xNO] surface intermediate that precedes the formation of surface N_2O [27]. At higher temperatures than 350 °C, the N_2O generation demonstrates the following order: SiO_x-promoted > unpromoted > ZrO_x-promoted > CeO_x-promoted. Correlation of N_2O generation and the strength of Brønsted acid sites above 350 °C, however, is not feasible due to the decreased intensity of the FTIR signals from adsorbed ammonia molecules at these elevated SCR reaction temperatures (Table S2).

Water Vapor-Containing SCR. The effect of water vapor on the SCR activity of the promoted catalysts are also illustrated in Fig. 4 by the dashed lines. The presence of water vapor significantly decreases NO conversion over the temperature range of 100–400 °C for all the catalysts, concurring with previous reports [19,20,25,26]. At 400 °C, the terminal V═O vibrations demonstrate redshifts of ~3–7 cm^{-1}, translating to 0.001–0.004 Å in the V═O bond lengths [85], for unpromoted, CeO_x-promoted, and ZrO_x-promoted catalysts compared to the dehydrated conditions (Fig. S3-S6). This suggests some perturbation of the surface V═O bonds by gas phase H_2O molecules. Thus, H_2O molecules compete with NH_3 and prevent them from interacting with the vanadia active sites, which is consistent with literature findings [5,18,19,23–26]. The NO conversion for unpromoted, promoted-SiO_x and promoted-ZrO_x catalysts reach their highest values at 500 °C (74 %, 67 %, and 56 %, respectively), instead of at 400 °C under *water vapor-free* SCR reaction conditions (Fig. 4a). The CeO_x-promoted catalyst, however, achieves the maximal NO conversion (88 %) at 400 °C before mildly decreasing to 77 % at 500 °C. The resulting order of NO conversion remains the same as that under the *water vapor-free* SCR environment: CeO_x-promoted > unpromoted > SiO_x-promoted > ZrO_x-promoted. The effect of over-oxidation of NH_3 is significantly suppressed, as indicated by the increase in NO conversion above 400 °C (Fig. 4a). Although water vapor does not impact the initial temperature of NO conversion, it delays N_2O generation by 50 °C for the CeO_x-promoted catalyst and 200 °C for SiO_x-promoted catalysts (Fig. 4c). Most significantly, the presence of 5 % H_2O significantly diminishes the generation of N_2O, which is attributed to decreased over-oxidation of NH_3 to N_2O (Fig. 4b). The over-oxidation of NH_3 to N_2O involves one NH_3 molecule, either NH_3* or NH_4^+*, and one NO molecule [27,86–88] and the lower surface concentration of ammonia in the presence of moisture most likely suppresses this bimolecular reaction. The order of N_2O formation exhibits the following trend: ZrO_x-promoted > unpromoted > CeO_x-promoted >> SiO_x-promoted in the 200–400 °C temperature range. This coincides with the order of the strength of Lewis acid sites discussed in the previous section: ZrO_x-promoted > unpromoted > CeO_x-promoted >> SiO_x-promoted. Previous work established that surface Lewis acid sites (NH_3*) are converted into surface Brønsted acid sites (NH_4^+*) under the influence of vapor water [16]. Considering this correlation between the strength of Lewis acid sites and N_2O generation, it is proposed that surface Lewis acid sites possess greater activity than surface Brønsted acid sites for N_2O formation on V_2O_5/TiO_2 catalysts.

3.6. Relationship between surface acid sites and activity of NO/NH_3 SCR reaction

Water Vapor-free NO/NH_3 SCR. Under the *water vapor-free* NO/NH_3 SCR reaction conditions, the unpromoted, SiO_x-promoted, and ZrO_x-promoted supported 1 % V_2O_5/TiO_2 catalysts exhibit comparable NO conversion activity in the 200–400 °C temperature range. The corresponding concentrations of surface Lewis acid sites, however, significantly vary for these catalysts (unpromoted > ZrO_x-promoted >> SiO_x-promoted). Furthermore, the SiO_x-promoted catalyst does not even possess any surface Lewis acid sites. The absence of a correlation between the SCR activity and concentration of surface Lewis acid sites indicates that the SCR activity doesn't strongly depend on the number of surface Lewis acid sites of the catalyst. Furthermore, the absence of surface Lewis acid sites on the SiO_x-promoted catalyst doesn't prevent the SCR reaction from proceeding on this catalyst. Similarly, for the surface Brønsted acid sites of the same three promoted catalysts, there is no correlation between NO conversion and concentration of surface Brønsted acid sites since the concentration of surface Brønsted acid sites is much greater for the SiO_x-promoted catalyst than the unpromoted and ZrO_x-promoted catalysts. The CeO_x-promoted catalyst has comparable surface concentrations of surface Lewis and Brønsted acid sites as the unpromoted and ZrO_x-promoted catalyst but is much more active for NO/NH_3 SCR because of the redox nature of CeO_x (present as either surface CeO_x sites and/or V-O-Ce bonds). In summary, there does not appear to be a clear relationship between the surface acid sites and the NO/NH_3 SCR activity since the acidic properties don't correlate with the SCR activity. The strength of surface Brønsted acid sites only correlates with the amount of produced N_2O, as discussed in Section 3.5.

Water Vapor-containing NO/NH_3 SCR. NO/NH_3 SCR. While the unpromoted, SiO_x-promoted, and ZrO_x-promoted supported 1 % V_2O_5/TiO_2 catalysts exhibit comparable SCR activity in the 200–400 °C temperature range, the SCR activities don't correlate with the number of surface Lewis and Brønsted acid sites. The unpromoted and ZrO_x-promoted catalysts have comparable numbers of surface Lewis acid sites and SCR activity, while the SiO_x-promoted catalyst doesn't possess surface Lewis acid sites and has the same SCR activity as the other two catalysts. The number of surface Brønsted acid sites for all the catalysts is comparable in the 200–400 °C temperature range, but the SCR activity varies over a large range with the CeO_x-promoted catalyst exhibiting much higher SCR activity. Thus, similar to the *water vapor-free* SCR reaction conditions, there does not appear to be a clear relationship between the surface acid sites and the NO/NH_3 SCR activity since the acidic properties don't correlate with the SCR activity. The strength of surface Lewis acid sites only correlates with the amount of produced N_2O, as discussed in Section 3.5, as a result of the interaction with moisture.

3.7. Relationship between concentration of surface monomers/dimers/oligomers and activity of NO/NH_3 SCR reaction

The fraction of dimer/oligomer surface VO_x sites demonstrate a slight increase from 68 % for the unpromoted 1 % V_2O_5/TiO_2 catalyst to 68–69 % for the ZrO_x- and SiO_x-promoted catalysts, respectively, and 73 % for the CeO_x-promoted catalyst. Additionally, the CeOx- and ZrO_x-promoted catalysts possess similar fractions of dimer and oligomer surface VO_x species (Table 1). Therefore, the comparable SCR activities for the unpromoted, SiO_x-, and ZrO_x-promoted catalysts and enhanced SCR activities for the CeO_x-promoted catalyst over the 200–400 °C temperature range, in the presence as well as absence of water vapor in the feed, suggest that, although the fraction of dimer/oligomer surface VO_x sites might be important for SCR activity [7,89], other factors ultimately drive the overall SCR activity for the vanadia-supported catalysts. One possible factor for the diverse SCR activity is that the surface VO_x sites are anchored to different surface hydroxyls and support ligands (Ti, Ce, Zr, Si) that are also known to exert a significant effect on

redox catalytic reactions [28,29,57,90,91]. Changing the specific oxide support ligand can alter the SCR TOFs by more than an order of magnitude [90], while a 40 % increase of the fraction of surface dimer/oligomer surface VO_x sites results in a merely 6-fold increase in the SCR TOF [7]. The enhanced SCR activity of the CeO_x-promoted catalyst, thus, is not related to the high fraction of surface dimer/-oligomer surface VO_x sites in the CeO_x-promoted catalyst but originates from the enhanced redox properties of the surface CeO_x sites (Fig. S13) and bridging V-O-Ce bonds in this catalyst.

4. Conclusions

The unpromoted and Ce-, Zr-, and Si-promoted supported 1 % V_2O_5/TiO_2 catalysts consisted of completely dispersed surface VO_x, CeO_x, ZrO_x, and SiO_x sites on the TiO_2 support. The surface VO_x sites anchored to both the surface hydroxyls of the TiO_2 support and the surface CeO_x, ZrO_x, and SiO_x sites. As a result, the surface PO_x promoters modified the (1) anchoring sites of VO_x on the surface modified TiO_2 support by forming V-O-P bonds, (2) surface Lewis and Brønsted acid properties of the supported V_2O_5/TiO_2 catalysts, but (3) did not significantly perturb the molecular structures of the surface VO_x sites (monomer, dimer, and oligomer). The presence of water vapor had a minimal effect on the molecular structures of the surface VO_x sites under the elevated SCR reaction conditions but generally increased the number of surface Brønsted acid sites. The presence of H_2O vapor, however, did compete with the adsorption of NH_3 and NO on the surface VO_x sites and, thus, decreased the formation of N_2O because of the lower surface concentration of adsorbed ammonia species. Among the promoters, the CeO_x-promoted catalyst significantly increased the SCR activity because of ceria's strong redox characteristic, both as surface CeO_x sites on the TiO_2 support and formation of bridging V-O-Ce bonds. The SiO_x- and ZrO_x-promoted catalysts, however, did not increase the SCR activity because of their low redox activity both as surface ZrO_x and SiO_x sites on TiO_2 and formation of and bridging V-O-ZrO_x and V-O-SiO_x bonds. These new molecular level insights provide a fundamental understanding of the role of promoter surface metal oxide sites on titania-supported vanadia catalysts and an effective strategy for the rational design of advanced SCR catalysts for the abatement of NO_x emissions. Additional insights into the surface hydroxyl anchoring sites, various bridging and terminal motifs, may be gained from solid-state ^{1}H MAS NMR and advanced DFT modeling.

CRediT authorship contribution statement

Qingling Liu: Supervision, Project administration, Funding acquisition. **Nicholas R. Jaegers:** Writing – review & editing, Supervision, Investigation. **Yong Wang:** Writing – review & editing, Supervision, Project administration, Funding acquisition. **Caixia Liu:** Supervision, Project administration, Funding acquisition. **Bar Mosevitzky Lis:** Writing – review & editing, Writing – original draft, Investigation. **Dinh Nhat Dang Nguyen:** Writing – review & editing, Writing – original draft, Visualization, Investigation. **Wenda Hu:** Writing – review & editing, Investigation. **Mingyu Guo:** Investigation. **Jian Zhi Hu:** Writing – review & editing, Supervision, Project administration, Funding acquisition. **Israel E. Wachs:** Writing – review & editing, Supervision, Project administration, Funding acquisition, Conceptualization.

Declaration of Competing Interest

The authors declare that they have no known competing financial interests or personal relationships that could have appeared to influence the work reported in this paper.

Acknowledgments

Research was primarily supported as part of Center for Understanding and Controlling Accelerated and Gradual Evolution of Materials for Energy (UNCAGE-ME), an Energy Frontier Research Center funded by the U.S. Department of Energy, Office of Science, Basic Energy Sciences under Award # DE-SC0012577 (catalyst synthesis, characterization, data analysis). The U.S. Department of Energy, Office of Basic Energy Sciences, Division of Chemical Sciences, Geosciences, and Biosciences within the Catalysis Science Program (FWP Award #47319) provided support for the NMR studies (solid-state 34 kHz ^{51}V MAS NMR experiments and data processing). In addition, investigator #3 acknowledges support by the National Natural Science Foundation of China (Award #52200128) and National Nonprofit Institute Research Grants of TIWTE (Award #TKS20230303) (steady state reaction studies).

Appendix A. Supporting information

Supplementary data associated with this article can be found in the online version at doi:10.1016/j.apcatb.2025.125942.

Data availability

Data will be made available on request.

References

[1] P. Forzatti, L. Lietti, Recent advances in De-NOxing catalysis for stationary applications, Heterog. Chem. Rev. 3 (1996) 33–51, https://doi.org/10.1002/(SICI)1234-985X(199603)3:1<33::AID-HCR54>3.0.CO;2-R.
[2] G. Busca, L. Lietti, G. Ramis, F. Berti, Chemical and mechanistic aspects of the selective catalytic reduction of NO by ammonia over oxide catalysts: a review, Appl. Catal. B. Environ. 18 (1998) 1–36, https://doi.org/10.1016/S0926-3373(98)00040-X.
[3] L. Lietti, J. Svachula, P. Forzatti, G. Busca, G. Ramis, P. Bregani, Surface and catalytic properties of Vanadia-Titania and Tungsta-Titania systems in the selective catalytic reduction of nitrogen oxides, Catal. Today 17 (1993) 131–139, https://doi.org/10.1016/0920-5861(93)80016-T.
[4] L. Han, S. Cai, M. Gao, J. Hasegawa, P. Wang, J. Zhang, L. Shi, D. Zhang, Selective catalytic reduction of NOx with NH3 by using novel catalysts: state of the art and future prospects, Chem. Rev. 119 (2019) 10916–10976, https://doi.org/10.1021/acs.chemrev.9b00202.
[5] J.-K. Lai, I.E. Wachs, A perspective on the selective catalytic reduction (SCR) of NO with NH3 by supported V2O5–WO3/TiO2 catalysts, ACS Catal. 8 (2018) 6537–6551, https://doi.org/10.1021/acscatal.8b01357.
[6] Y. He, M.E. Ford, M. Zhu, Q. Liu, U. Tumuluri, Z. Wu, I.E. Wachs, Influence of catalyst synthesis method on selective catalytic reduction (SCR) of NO by NH3 with V2O5-WO3/TiO2 catalysts, Appl. Catal. B 193 (2016) 141–150, https://doi.org/10.1016/j.apcatb.2016.04.022.
[7] N.R. Jaegers, J. Lai, Y. He, E. Walter, D.A. Dixon, M. Vasiliu, Y. Chen, C. Wang, M. Y. Hu, K.T. Mueller, I.E. Wachs, Y. Wang, J.Z. Hu, Mechanism by which tungsten oxide promotes the activity of supported V2O5/TiO2 catalysts for NOx abatement: structural effects revealed by 51V MAS NMR spectroscopy, Angew. Chem. Int. Ed. 131 (2019) 12739–12746, https://doi.org/10.1002/ange.201904503.
[8] M.A. Vuurman, I.E. Wachs, A.M. Hirt, Structural determination of supported V2O5-WO3/TiO2 catalysts by in situ Raman spectroscopy and X-ray photoelectron spectroscopy, J. Phys. Chem. 95 (1991) 9928–9931.
[9] L.J. Alemany, F. Berti, G. Busca, G. Ramis, D. Robba, G.Pietro Toledo, M. Trombetta, Characterization and composition of commercial V2O5-WO3-TiO2 SCR catalysts, Appl. Catal. B. Environ. 10 (1996) 299–311, https://doi.org/10.1016/S0926-3373(96)00032-X.
[10] M.D. Amiridis, I.E. Wachs, G. Deo, J.-M. Jehng, D.S. Kim, Reactivity of V2O5 catalysts for the selective catalytic reduction of NO by NH3: influence of vanadia loading, H2O, and SO2, J. Catal. 161 (1996) 247–253, https://doi.org/10.1006/jcat.1996.0182.
[11] M. Waqif, J. Bachelier, O. Saur, J.-C. Lavalley, Acidic properties and stability of Sulfate-promoted metal oxides, J. Mol. Catal. 72 (1992) 127–138, https://doi.org/10.1016/0304-5102(92)80036-G.
[12] M. Zhu, J.-K. Lai, U. Tumuluri, M.E. Ford, Z. Wu, I.E. Wachs, Reaction pathways and kinetics for selective catalytic reduction (SCR) of acidic NOx emissions from power plants with NH3, ACS Catal. 7 (2017) 8358–8361, https://doi.org/10.1021/acscatal.7b03149.
[13] R.Y. Saleh, I.E. Wachs, S.S. Chan, C.C. Chersich, the interaction of V2O5 with Ti02 (anatase): catalyst evolution with calcination temperature and O-xylene oxidation, J. Catal. 98 (1986) 102–114, https://doi.org/10.1016/0021-9517(86)90300-3.
[14] J.P. Dunn, H.G. Stenger, I.E. Wachs, Oxidation of sulfur dioxide over supported vanadia catalysts: molecular structure – reactivity relationships and reaction kinetics, Catal. Today 51 (1999) 301–318, https://doi.org/10.1016/S0920-5861(99)00052-8.

[15] L. Lietti, J.L. Alemany, P. Forzatti, G. Busca, G. Ramis, E. Giamello, F. Bregani, Reactivity of V2O5-WO3/TiO2 catalysts in the selective catalytic reduction of nitric oxide by ammonia, Catal. Today 29 (1996) 143–148, https://doi.org/10.1016/0920-5861(95)00250-2.
[16] M. Zhu, J.-K. Lai, U. Tumuluri, Z. Wu, I.E. Wachs, Nature of active sites and surface intermediates during SCR of NO with NH3 by supported V2O5–WO3/TiO2 catalysts, J. Am. Chem. Soc. 139 (2017) 15624–15627, https://doi.org/10.1021/jacs.7b09646.
[17] C. Song, W. Pan, S.T. Srimat, J. Zheng, Y. Li, Y.-H. Wang, B.-Q. Xu, Q.-M. Zhu, Tri-reforming of methane over ni catalysts for CO2 conversion to syngas with desired H2/CO ratios using flue gas of power plants without CO2 separation, Stud. Surf. Sci. Catal. 153 (2004) 315–322, https://doi.org/10.1016/S0167-2991(04)80270-2.
[18] L. Lietti, I. Nova, P. Forzatti, Selective catalytic reduction (SCR) of NO by NH3 over TiO2-supported V2O5–WO3 and V2O5–MoO3 catalysts, Top. Catal. 11/12 (2000) 111–122, https://doi.org/10.1023/A:1027217612947.
[19] R. Gui, Q. Yan, T. Xue, Y. Gao, Y. Li, T. Zhu, Q. Wang, The Promoting/Inhibiting effect of water vapor on the selective catalytic reduction of NOx, J. Hazard. Mater. 439 (2022) 129665, https://doi.org/10.1016/j.jhazmat.2022.129665.
[20] N.-Y. ToPsøE, T. Slabiak, B.S. Clausen, T.Z. Srnak, J.A. Dumesic, Influence of water on the reactivity of Vanadia/Titania for catalytic reduction of NOx, J. Catal. 134 (1992) 742–746, https://doi.org/10.1016/0021-9517(92)90358-O.
[21] P. Forzatti, Environmental catalysis for stationary applications, Catal. Today 62 (2000) 51–65, https://doi.org/10.1016/S0920-5861(00)00408-9.
[22] I. Nova, L. Lietti, E. Tronconi, P. Forzatti, Transient response method applied to the kinetic analysis of the DeNOx–SCR reaction, Chem. Eng. Sci. 56 (2001) 1229–1237, https://doi.org/10.1016/S0009-2509(00)00344-4.
[23] P. Forzatti, Present status and perspectives in de-NOx SCR catalysis, Appl. Catal. A. Gen. 222 (2001) 221–236, https://doi.org/10.1016/S0926-860X(01)00832-8.
[24] M. Turco, L. Lisi, R. Pirone, P. Ciambelli, Effect of water on the kinetics of nitric oxide reduction over a High-Surface-Area V2O5/TiO2 catalyst, Appl. Catal. B. Environ. 3 (1994) 133–149, https://doi.org/10.1016/0926-3373(94)80001-4.
[25] J.A. Dumesic, N.-Y. Topsøe, H. Topsøe, Y. Chen, T. Slabiak, Kinetics of selective catalytic reduction of nitric oxide by ammonia over Vanadia/Titania, J. Catal. 163 (1996) 409–417, https://doi.org/10.1006/jcat.1996.0342.
[26] H.-G. Lintz, T. Turek, Intrinsic kinetics of nitric oxide reduction by ammonia on a Vanadia-Titania catalyst, Appl. Catal. A. Gen. 85 (1992) 13–25, https://doi.org/10.1016/0926-860X(92)80126-W.
[27] M. Zhu, J.-K. Lai, I.E. Wachs, Formation of N2O greenhouse gas during SCR of NO with NH3 by supported vanadium oxide catalysts, Appl. Catal. B. Environ. 224 (2018) 836–840, https://doi.org/10.1016/j.apcatb.2017.11.029.
[28] M. Guo, B. Mosevitzky Lis, M.E. Ford, I.E. Wachs, Effect of redox promoters (CeOx and CuOx) and surface sulfates on the selective catalytic reduction (SCR) of NO with NH3 by supported V2O5-WO3/TiO2 catalysts, Appl. Catal. B. Environ. 306 (2022) 121108, https://doi.org/10.1016/j.apcatb.2022.121108.
[29] M. Guo, B. Mosevitzky Lis, M.E. Ford, I.E. Wachs, The effect of non-redox promoters (AlOx, POx, SiOx and ZrOx) and surface sulfates on supported V2O5-WO3/TiO2 catalysts in selective catalytic reduction of NO with NH3, Appl. Catal. B. Environ. 306 (2022) 121128, https://doi.org/10.1016/j.apcatb.2022.121128.
[30] D. Wang, Y. Peng, Q. Yang, F. Hu, J. Li, J. Crittenden, NH3-SCR performance of WO3 blanketed CeO2 with different morphology: balance of surface reducibility and acidity, Catal. Today 332 (2019) 42–48, https://doi.org/10.1016/j.cattod.2018.07.048.
[31] A. Shi, X. Wang, T. Yu, M. Shen, The effect of zirconia additive on the activity and structure stability of V2O5/WO3-TiO2 ammonia SCR catalysts, Appl. Catal. B. Environ. 106 (2011) 359–369, https://doi.org/10.1016/j.apcatb.2011.05.040.
[32] Z. Yan, W. Shan, X. Shi, G. He, Z. Lian, Y. Yu, Y. Shan, J. Liu, H. He, The way to enhance the thermal stability of V2O5-Based catalysts for NH3-SCR, Catal. Today 355 (2020) 408–414, https://doi.org/10.1016/j.cattod.2019.07.037.
[33] L. Chen, J. Li, M. Ge, Promotional effect of Ce-doped V2O5-WO3/TiO2 with low vanadium loadings for selective catalytic reduction of NOx by NH3, J. Phys. Chem. C. 113 (2009) 21177–21184, https://doi.org/10.1021/jp907109e.
[34] K.A. Michalow-Mauke, Y. Lu, K. Kowalski, T. Graule, M. Nachtegaal, O. Kröcher, D. Ferri, Flame-Made WO3/CeOx-TiO2 catalysts for selective catalytic reduction of NOx by NH3, ACS Catal. 5 (2015) 5657–5672, https://doi.org/10.1021/acscatal.5b01580.
[35] B.M. Reddy, A. Khan, Y. Yamada, T. Kobayashi, S. Loridant, J.-C. Volta, Structural characterization of CeO2 −TiO2 and V2O5/CeO2 −TiO2 catalysts by Raman and XPS techniques, J. Phys. Chem. B. 107 (2003) 5162–5167, https://doi.org/10.1021/jp0344601.
[36] X. Liu, X. Wu, T. Xu, D. Weng, Z. Si, R. Ran, Effects of silica additive on the NH3-SCR activity and thermal stability of a V2O5/WO3-TiO2 catalyst, Chin. J. Catal. 37 (2016) 1340–1346, https://doi.org/10.1016/S1872-2067(15)61109-3.
[37] A. Marberger, D. Ferri, D. Rentsch, F. Krumeich, M. Elsener, O. Kröcher, Effect of SiO2 on Co-impregnated V2O5/WO3/TiO2 catalysts for the selective catalytic reduction of NO with NH3, Catal. Today 320 (2019) 123–132, https://doi.org/10.1016/j.cattod.2017.11.037.
[38] X. Liu, H. Chen, X. Wu, L. Cao, P. Jiang, Q. Yu, Y. Ma, Effects of SiO2 modification on the hydrothermal stability of the V2O5/WO3–TiO2 NH3-SCR catalyst: TiO2 structure and vanadia species, Catal. Sci. Technol. 9 (2019) 3711–3720, https://doi.org/10.1039/C9CY00385A.
[39] X.-Z. Shao, H.-Y. Wang, M.-L. Yuan, J. Yang, W.-C. Zhan, L. Wang, Y. Guo, G.-Z. Lu, Thermal stability of Si-doped V2O5/WO3–TiO2 for selective catalytic reduction of NOx by NH3, Rare Met. 38 (2019) 292–298, https://doi.org/10.1007/s12598-018-1176-x.
[40] Y. Pan, W. Zhao, Q. Zhong, W. Cai, H. Li, Promotional effect of Si-doped V2O5/TiO2 for selective catalytic reduction of NOx by NH3, J. Environ. Sci. 25 (2013) 1703–1711, https://doi.org/10.1016/S1001-0742(12)60181-8.
[41] R. JOSSEN, M. HEINE, S. PRATSINIS, S. AUGUSTINE, M. AKHTAR, Thermal stability and catalytic activity of flame-made silica–vanadia–tungsten oxide–titania, Appl. Catal. B. Environ. 69 (2007) 181–188, https://doi.org/10.1016/j.apcatb.2006.06.018.
[42] H. Eckert, I.E. Wacjs, ^{51}V NMR: a new probe of structure and bonding in catalysts, MRS Proc. 111 (1987) 459, https://doi.org/10.1557/PROC-111-459.
[43] H. Eckert, I.E. Wachs, Solid-state vanadium-51 NMR structural studies on supported vanadium(V) oxide catalysts: vanadium oxide surface layers on alumina and titania supports, J. Phys. Chem. 93 (1989) 6796–6805, https://doi.org/10.1021/j100355a043.
[44] H. Eckert, G. Deo, I.E. Wachs, A.M. Hirt, Solid state ^{51}V NMR structural studies of vanadium(V) oxide catalysts supported on TiO2(anatase) and TiO2(rutile). the influence of surface impurities on the vanadium(V) coordination, Colloids Surf. 45 (1990) 347–359, https://doi.org/10.1016/0166-6622(90)80036-4.
[45] C. Femandez, M. Guelton, Chapter 5.1 characterization of V2O5/TiO2 catalysts by solid state NMR of 51V, Catal. Today 20 (1994) 77–86, https://doi.org/10.1016/0920-5861(94)85017-8.
[46] L.G. Pinaeva, O.B. Lapina, V.M. Mastikhin, A.V. Nosov, B.S. Balzhinimaev, 1H and 51V high-resolution solid state nuclear magnetic resonance studies of supported V2O5/TiO2 catalysts, J. Mol. Catal. 88 (1994) 311–323, https://doi.org/10.1016/0304-5102(93)E0277-N.
[47] A. Burkardt, W. Weisweiler, J.A.A. van den Tillaart, A. Schäfer-Sindlinger, E.S. Lox, Influence of the V2O5 loading on the structure and activity of V2O5/TiO2 SCR catalysts for vehicle application, Top. Catal. 16/17 (2001) 369–375, https://doi.org/10.1023/A:1016673418398.
[48] U.G. Nielsen, N.-Y. Topsøe, M. Brorson, J. Skibsted, H.J. Jakobsen, The complete 51V MAS NMR spectrum of surface vanadia nanoparticles on anatase (TiO2): vanadia surface structure of a DeNOx catalyst, J. Am. Chem. Soc. 126 (2004) 4926–4933, https://doi.org/10.1021/ja030091a.
[49] N.R. Jaegers, Y. Wang, J.Z. Hu, I.E. Wachs, Impact of hydration on supported V2O5/TiO2 catalysts as explored by magnetic resonance spectroscopy, J. Phys. Chem. C. 125 (2021) 16766–16775, https://doi.org/10.1021/acs.jpcc.1c04150.
[50] I.E. Wachs, C.J. Keturakis, Monolayer systems. in: Comprehensive Inorganic Chemistry II, Elsevier, 2013, pp. 131–151, https://doi.org/10.1016/B978-0-08-097774-4.00717-8.
[51] H. Zhu, M. Shen, Y. Kong, J. Hong, Y. Hu, T. Liu, L. Dong, Y. Chen, C. Jian, Z. Liu, Characterization of copper oxide supported on Ceria-Modified anatase, J. Mol. Catal. A. Chem. 219 (2004) 155–164, https://doi.org/10.1016/j.molcata.2004.04.032.
[52] J.-M. Jehng, I.E. Wachs, B.M. Weckhuysen, R.A. Schoonheydt, Surface chemistry of Silica–Titania-Supported chromium oxide catalysts, J. Chem. Soc. Faraday Trans. 91 (1995) 953–961, https://doi.org/10.1039/FT9959100953.
[53] N. Katada, M. Niwa, Y. Murakami, Acidic property of silica monolayers on metal oxides prepared by CVD method, in: Elsevier, 1994, pp. 333–338, https://doi.org/10.1016/S0167-2991(08)61842-X.
[54] I.E. Wachs, J.-M. Jehng, G. Deo, B.M. Weckhuysen, V.V. Guliants, J.B. Benziger, S. Sundaresan, Fundamental studies of butane oxidation over Model-Supported vanadium oxide catalysts: molecular Structure-Reactivity relationships, J. Catal. 170 (1997) 75–88, https://doi.org/10.1006/jcat.1997.1742.
[55] C. Deiana, E. Fois, S. Coluccia, G. Martra, Surface structure of TiO2 P25 nanoparticles: infrared study of hydroxy groups on coordinative defect sites, J. Phys. Chem. C. 114 (2010) 21531–21538, https://doi.org/10.1021/jp107671k.
[56] O.B. Lapina, D.F. Khabibulin, A.A. Shubin, E. Papulovskiy, V.V. Terskikh, I. E. Wachs, Structure and reactivity of surface vanadia sites in bi-layered supported VOx/AlOx/SiO2 catalysts via solid-state NMR, first-principles calculations, and catalytic studies, Catal. Today 441 (2024) 114880, https://doi.org/10.1016/j.cattod.2024.114880.
[57] I.E. Wachs, B.M. Weckhuysen, Structure and reactivity of surface vanadium oxide species on oxide supports, Appl. Catal. A. Gen. 157 (1997) 67–90, https://doi.org/10.1016/S0926-860X(97)00021-5.
[58] E.I. Ross-Medgaarden, I.E. Wachs, W.V. Knowles, A. Burrows, C.J. Kiely, M. S. Wong, Tuning the electronic and molecular structures of catalytic active sites with titania nanoligands, J. Am. Chem. Soc. 131 (2009) 680–687, https://doi.org/10.1021/ja711456c.
[59] C. Schilling, A. Hofmann, C. Hess, M.V. Ganduglia-Pirovano, Raman spectra of polycrystalline CeO2: a density functional theory study, J. Phys. Chem. C. 121 (2017) 20834–20849, https://doi.org/10.1021/acs.jpcc.7b06643.
[60] E.L. Lee, I.E. Wachs, In situ Raman spectroscopy of SiO2-Supported transition metal oxide catalysts: an isotopic 18O− 16O exchange study, J. Phys. Chem. C. 112 (2008) 6487–6498, https://doi.org/10.1021/jp076485w.
[61] M.A. Sliem, D.A. Schmidt, A. Bétard, S.B. Kalidindi, S. Gross, M. Havenith, A. Devi, R.A. Fischer, Surfactant-Induced nonhydrolytic synthesis of Phase-Pure ZrO2 nanoparticles from metal–organic and oxocluster precursors, Chem. Mater. 24 (2012) 4274–4282, https://doi.org/10.1021/cm301128a.
[62] P. Ji, Z. Mao, Z. Wang, X. Xue, Y. Zhang, J. Lv, X. Shi, Improved surface-enhanced Raman scattering properties of ZrO2 nanoparticles by zn doping, Nanomaterials 9 (2019) 983, https://doi.org/10.3390/nano9070983.
[63] R.J.G. Nuguid, D. Ferri, A. Marberger, M. Nachtegaal, O. Kröcher, Modulated excitation Raman spectroscopy of V2O5/TiO2: mechanistic insights into the selective catalytic reduction of NO with NH3, ACS Catal. 9 (2019) 6814–6820, https://doi.org/10.1021/acscatal.9b01514.
[64] F. Roozeboom, M.C. Mittelmeijer-Hazeleger, J.A. Moulijn, J. Medema, V.H.J. De Beer, P.J. Gellings, Vanadium oxide monolayer catalysts. 3. a Raman spectroscopic

and Temperature-Programmed reduction study of monolayer and Crystal-Type vanadia on various supports, J. Phys. Chem. 84 (1980) 2783–2791, https://doi.org/10.1021/j100458a023.
[65] G.T. Went, S. Ted. Oyama, A.T. Bell, Laser Raman spectroscopy of supported vanadium oxide catalysts, J. Phys. Chem. 94 (1990) 4240–4246, https://doi.org/10.1021/j100373a067.
[66] I. Giakoumelou, C. Fountzoula, C. Kordulis, S. Boghosian, Molecular structure and catalytic activity of V2O5/TiO2 catalysts for the SCR of NO by NH3: in situ Raman spectra in the presence of O2, NH3, NO, H2, H2O, and SO2, J. Catal. 239 (2006) 1–12, https://doi.org/10.1016/j.jcat.2006.01.019.
[67] J. Matta, D. Courcot, E. Abi-Aad, A. Aboukaïs, Identification of vanadium oxide species and trapped single electrons in interaction with the CeVO4 phase in Vanadium−Cerium oxide systems. 51V MAS NMR, EPR, Raman, and thermal analysis studies, Chem. Mater. 14 (2002) 4118–4125, https://doi.org/10.1021/cm010396t.
[68] M. Ying, J. Hou, W. Xie, Y. Xu, S. Shen, H. Pan, M. Du, Synthesis, semiconductor characteristics and Gas-Sensing selectivity for Cerium-Doped neodymium vanadate nanorods, Sens. Actuators B. Chem. 260 (2018) 125–133, https://doi.org/10.1016/j.snb.2017.12.192.
[69] W. Wei, Q. Gao, J. Guo, M. Chao, L. He, J. Chen, E. Liang, Realizing isotropic negative thermal expansion covering room temperature by breaking the superstructure of ZrV2O7, Appl. Phys. Lett. 116 (2020) 181902, https://doi.org/10.1063/1.5143691.
[70] J.Z. Hu, S. Xu, W.-Z. Li, M.Y. Hu, X. Deng, D.A. Dixon, M. Vasiliu, R. Craciun, Y. Wang, X. Bao, C.H.F. Peden, Investigation of the structure and active sites of TiO2 nanorod supported VOx catalysts by High-Field and Fast-Spinning 51V MAS NMR, ACS Catal. 5 (2015) 3945–3952, https://doi.org/10.1021/acscatal.5b00286.
[71] J. Matta, D. Courcot, E. Abi-Aad, A. Aboukaïs, Identification of vanadium oxide species and trapped single electrons in interaction with the CeVO4 phase in Vanadium−Cerium oxide systems. 51V MAS NMR, EPR, Raman, and thermal analysis studies, Chem. Mater. 14 (2002) 4118–4125, https://doi.org/10.1021/cm010396t.
[72] N.R. Jaegers, C. Wan, M.Y. Hu, M. Vasiliu, D.A. Dixon, E. Walter, I.E. Wachs, Y. Wang, J.Z. Hu, Investigation of Silica-Supported vanadium oxide catalysts by High-Field 51V Magic-Angle spinning NMR, J. Phys. Chem. C. 121 (2017) 6246–6254, https://doi.org/10.1021/acs.jpcc.7b01658.
[73] J.T. Grant, C.A. Carrero, A.M. Love, R. Verel, I. Hermans, Enhanced two-dimensional dispersion of group v metal oxides on silica, ACS Catal. 5 (2015) 5787–5793, https://doi.org/10.1021/acscatal.5b01679.
[74] J.-M. Jehng, G. Deo, B.M. Weckhuysen, I.E. Wachs, Effect of water vapor on the molecular structures of supported vanadium oxide catalysts at elevated temperatures, J. Mol. Catal. A. Chem. 110 (1996) 41–54, https://doi.org/10.1016/1381-1169(96)00061-1.
[75] M. Avramovska, D. Freude, J. Haase, A.V. Toktarev, S.S. Arzumanov, A. A. Gabrienko, A.G. Stepanov, Quantitative 67Zn, 27Al and 1H MAS NMR spectroscopy for the characterization of zn species in ZSM-5 catalysts, Phys. Chem. Chem. Phys. 25 (2023) 28043–28051, https://doi.org/10.1039/D3CP03136E.
[76] A.L. Paterson, Quadrupolar Quantitative Bloch Decay v1, (2024). https://doi.org/10.17504/protocols.io.n2bvjn9wngk5/v1.
[77] M.M. Mason, I.E. Wachs, D.A. Dixon, Assignment of vibrational bands of critical surface species containing nitrogen in the selective catalytic reduction of NO by NH3, J. Phys. Chem. A. 127 (2023) 240–249, https://doi.org/10.1021/acs.jpca.2c08580.
[78] D.C. McKean, P.N. Schatz, Absolute infrared intensities of vibration bands in ammonia and phosphine, J. Chem. Phys. 24 (1956) 316–325, https://doi.org/10.1063/1.1742470.
[79] T.H. Koops, T. Visser, W.M.A. Smit, Measurement and interpretation of the absolute infrared intensities of NH3 and ND3, J. Mol. Struct. 96 (1983) 203–218, https://doi.org/10.1016/0022-2860(83)90049-2.
[80] E.R. Keim, M.L. Polak, J.C. Owrutsky, J.V. Coe, R.J. Saykally, Absolute infrared vibrational band intensities of molecular ions determined by direct laser absorption spectroscopy in fast ion beams, J. Chem. Phys. 93 (1990) 3111–3119, https://doi.org/10.1063/1.458845.
[81] Z. Ma, X. Wu, Y. Feng, Z. Si, D. Weng, L. Shi, Low-Temperature SCR activity and SO2 deactivation mechanism of Ce-Modified V2O5–WO3/TiO2 catalyst, Prog. Nat. Sci. Mater. Int. 25 (2015) 342–352, https://doi.org/10.1016/j.pnsc.2015.07.002.
[82] J. Arfaoui, A. Ghorbel, C. Petitto, G. Delahay, Novel V2O5-CeO2-TiO2-SO42−Nanostructured aerogel catalyst for the low temperature selective catalytic reduction of NO by NH3 in excess O2, Appl. Catal. B. Environ. 224 (2018) 264–275, https://doi.org/10.1016/j.apcatb.2017.10.059.
[83] T.H. Vuong, J. Radnik, J. Rabeah, U. Bentrup, M. Schneider, H. Atia, U. Armbruster, W. Grünert, A. Brückner, Efficient VOx/Ce1–x TixO2 catalysts for low-temperature NH3-SCR: reaction mechanism and active sites assessed by in Situ/Operando spectroscopy, ACS Catal. 7 (2017) 1693–1705, https://doi.org/10.1021/acscatal.6b03223.
[84] D. Ye, R. Qu, S. Liu, C. Zheng, X. Gao, New insights into the decomposition behavior of NH4HSO4 on the SiO2-Decorated SCR catalyst and its enhanced SO2-Resistant ability, ACS Omega 4 (2019) 4927–4935, https://doi.org/10.1021/acsomega.8b03128.
[85] F.D. Hardcastle, I.E. Wachs, Determination of vanadium-oxygen bond distances and bond orders by Raman spectroscopy, J. Phys. Chem. 95 (1991) 5031–5041, https://doi.org/10.1021/j100166a025.
[86] F.J.J.G. Janssen, F.M.G. Van den Kerkhof, Hans Bosch, J.R.H. Ross, Mechanism of the reaction of nitric oxide, ammonia, and oxygen over vanadia catalysts. 2. isotopic transient studies with oxygen-18 and nitrogen-15, J. Phys. Chem. 91 (1987) 6633–6638, https://doi.org/10.1021/j100311a016.
[87] U.S. Ozkan, M.W. Kumthekar, Y.P. Cai, Selective catalytic reduction of nitric oxide over Vanadia/Titania catalysts: temperature-programmed desorption and isotopically labeled oxygen-exchange studies, Ind. Eng. Chem. Res. 33 (1994) 2924–2929, https://doi.org/10.1021/ie00036a005.
[88] U.S. Ozkan, Y. Cai, M.W. Kumthekar, Mechanistic studies of selective catalytic reduction of nitric oxide with ammonia over V2O5/TiO2 (anatase) catalysts through transient isotopic labeling at steady state, J. Phys. Chem. 99 (1995) 2363–2371, https://doi.org/10.1021/j100008a019.
[89] G.T. Went, L.-J. Leu, R.R. Rosin, A.T. Bell, The effects of structure on the catalytic activity and selectivity of V2O5/TiO2 for the reduction of NO by NH3, J. Catal. 134 (1992) 492–505, https://doi.org/10.1016/0021-9517(92)90337-H.
[90] I.E. Wachs, G. Deo, B.M. Weckhuysen, A. Andreini, M.A. Vuurman, M. de Boer, M. D. Amiridis, Selective catalytic reduction of NO with NH3over supported vanadia catalysts, J. Catal. 161 (1996) 211–221, https://doi.org/10.1006/jcat.1996.0179.
[91] J.P. Dunn, P.R. Koppula, H. G. Stenger, I.E. Wachs, Oxidation of sulfur dioxide to sulfur trioxide over supported vanadia catalysts, Appl. Catal. B. Environ. 19 (1998) 103–117, https://doi.org/10.1016/S0926-3373(98)00060-5.